Phase resolved observation of spin wave modes in antidot lattices

View Online   Export Citation   CrossMark

Felix Groß,[1,a)] Mateusz Zelent,[2] Ajay Gangwar,[3] Sławomir Mamica,[2] Paweł Gruszecki,[2] Matthias Werner,[1]
Gisela Schütz,[1] Markus Weigand,[4] Eberhard J. Goering,[1] Christian H. Back,[5] Maciej Krawczyk,[2]
and Joachim Gräfe[1,a)]

AFFILIATIONS

[1]Max Planck Institute for Intelligent Systems, 70569 Stuttgart, Germany
[2]Faculty of Physics, Adam Mickiewicz University, Poznań, 61-614 Poznań, Poland
[3]Department of Physics, University of Regensburg, 93053 Regensburg, Germany
[4]Helmholtz-Zentrum Berlin für Materialien und Energie, 12489 Berlin, Germany
[5]Technical University Munich, 85748 Garching, Germany

Note: This paper is part of the APL Special Collection on Mesoscopic Magnetic Systems: From Fundamental Properties to Devices.
[a)]Authors to whom correspondence should be addressed: fgorss@is.mpg.de and graefe@is.mpg.de

ABSTRACT

Antidot lattices have proven to be a powerful tool for spin wave band structure manipulation. Utilizing time-resolved scanning transmission x-ray microscopy, we are able to experimentally image edge-localized spin wave modes in an antidot lattice with a lateral confinement down to <80 nm $\times$ 130 nm. At higher frequencies, spin wave dragonfly patterns formed by the demagnetizing structures of the antidot lattice are excited. Evaluating their relative phase with respect to the propagating mode within the antidot channel reveals that the dragonfly modes are not directly excited by the antenna but need the propagating mode as an energy mediator. Furthermore, micromagnetic simulations reveal that additional dispersion branches exist for a tilted external field geometry. These branches correspond to asymmetric spin wave modes that cannot be excited in a non-tilted field geometry due to the symmetry restriction. In addition to the band having a negative slope, these asymmetric modes also cause an unexpected transformation of the band structure, slightly reaching into the otherwise empty bandgap between the low frequency edge modes and the fundamental mode. The presented phase resolved investigation of spin waves is a crucial step for spin wave manipulation in magnonic crystals.

Magnonics, i.e., the manipulation of spin waves on the nanoscale, is an advancing field of interest that is analogous to photonics, which addresses the manipulation of light.[1–3] What makes magnonics even more fascinating is the intrinsic symmetry breaking in a uniform magnetic thin film due to the dipolar interaction depending on the relative orientation of magnetization and wave vector of the spin wave. However, this simultaneously enriches magnonic devices by allowing for the coexistence of various magnetostatic spin wave modes with different k-vector orientations.[4,5]

While challenging to handle, this particular complexity also offers unique possibilities to influence and observe spin waves on the scale of their own wavelength.[2] Modern nanostructuring techniques allow to engineer artificial magnonic structures in the sub-micrometer regime,[6–10] while time-resolved scanning transmission x-ray microscopy (TR-STXM) offers high spatial and temporal resolution[5,11–14] and hence allows for the direct observation of ultra-fast dynamics on the nanoscale.

One type of artificial magnonic crystals is two dimensional antidot lattices, i.e., periodic arrangements of holes in ferromagnetic thin films that cause periodic variations of saturation magnetization and demagnetization fields. Just like for electronic crystals, this periodic spin wave potential leads to the formation of a band structure for spin waves.[2,3,15–19] A characteristic peculiarity of these systems is so-called edge modes that are localized in the vicinity of the antidot edges. Here, the magnetization exhibits the strongest perturbations caused by the demagnetization fields.[20–26]

Such edge modes derive from magnetostatic spin wave modes but are trapped in the potential wells created by the local minima of

the effective field.[27–30] Nevertheless, these modes were rarely experimentally observed, since depending on the lattice constant, their lateral confinement can exceed the resolution of optical measurement methods,[2,16,20,31] and only a few measurements of edge modes have been published so far.[31–35] Thus, the description of antidot lattices relies mainly on micromagnetic simulations.[20,36] There are indications for several types of these localized edge modes,[20] however, their fundamental nature and coexitence with propagating modes remain experimentally unexplored,[20,25,33] but exist, as we will show.

In this article, we present a combination of STXM measurements and simulations to investigate multiple modes existing in antidot lattices. First, we will discuss the amplitude and phase distribution of propagating modes and edge modes. Furthermore, dragonfly like modes induced by the demagnetizing structure will be investigated. Additionally, we illustrate higher order standing spin waves and complement our findings with micromagnetic simulations allowing us to analyze additional modes, which are only excited in a tilted field geometry.

To observe the spin wave propagation in antidot lattices, 50 nm thin Py films were deposited on Si_3N_4 membranes. The antidot lattice includes holes of diameter $d = 450$ nm with a center to center distance $a = 900$ nm. For radio frequency (RF) excitation, a 2 μm wide antenna was structured on top of the Permalloy. An example of the sample design is sketched in Fig. 1(a).

Simulations[37] were performed with a damping coefficient of $\alpha = 1 \times 10^{-6}$ to extend the propagation distance of spin waves in order to obtain high resolution dispersion relations. The saturation magnetization and exchange constant were set to $M_s = 6 \times 10^5$ A/m and $A_{ex} = 13 \times 10^{-12}$ J/m, respectively, to qualitatively match simulations with experimental results. To keep the simulations as close to the experiment as possible, the spin waves were excited by a locally oscillating field to imitate a microstrip antenna. Periodic boundary conditions were used in order to simulate a continuous thin film. In order to calculate the dispersion relation, we used a temporal and spatial fast Fourier transformation to obtain the amplitude for a given frequency and k-vector. To obtain simulated real space images, the inverse Fourier transformation was applied to all k-vector components of a particular frequency.

Time resolved STXM measurements were conducted at the MAXYMUS end station of the UE46-PGM2 beam line at the BESSY II synchrotron radiation facility. The samples were illuminated under perpendicular incidence of circularly polarized light in an applied in-plane field of up to 240 mT generated by a set of four rotatable permanent magnets.[38] The photon energy was set to the absorption maximum of the Fe L_3 edge to get optimal x-ray magnetic circular dichroism contrast for imaging. A lock-in like detection scheme allows for RF excitation at arbitrary frequencies at a temporal resolution of 50 ps. This method allows for the pixel-wise recording of spin wave movies in real space and time domain. A subsequent temporal fast Fourier transformation allows for frequency filtering. For more information on TR-STXM for spin wave measurements, the reader is referred elsewhere.[5,11,12]

The simulated dispersion relation shows characteristics of magnonic crystal band structures and reveals that there are multiple modes existing at different frequencies. As illustrated in the dispersion relation in Fig. 1(b), depending on the frequency either edge modes, the fundamental Damon–Eshbach mode or higher order modes are
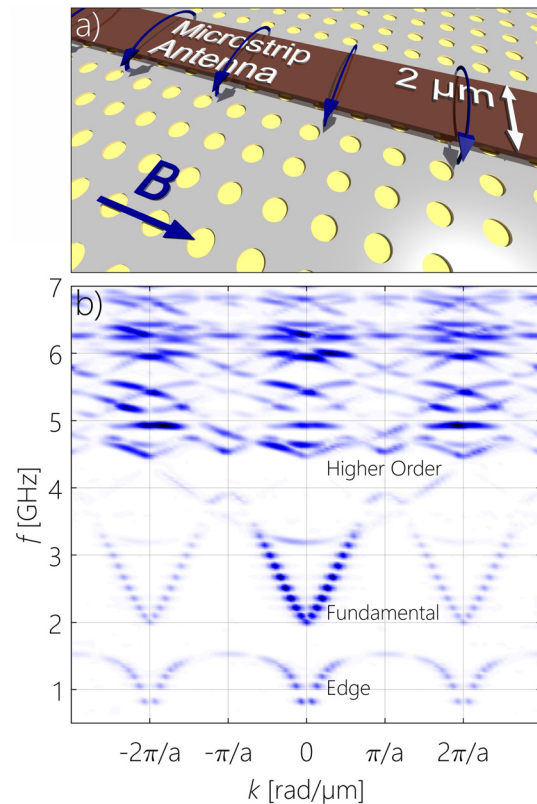
FIG. 1. (a) Sketch of an antidot lattice sample for x-ray microscopy. 50 nm of Permalloy (gray) are deposited on top of the x-ray transparent Si_3N_4 membrane (yellow). For spin wave excitation, a 2 μm wide copper antenna (brown) is deposited on top of the magnetic thin film. An external field is applied along the direction of the microstrip antenna. (b) Simulated spin wave dispersion relation for an applied field of 25 mT.

excited by the microstrip antenna. As seen in the dispersion relation, the higher order modes at high frequencies experience hybridization and exhibit multiple k-vectors coexisting at the same frequency within a single Brillouin zone.

In the following discussion, we will start with lower frequencies' edge modes and increase the excitation frequency as we advance in the manuscript. First, we analyze the amplitude and phase of experimentally measured edge modes. Increasing the frequency allows to observe the fundamental mode and its interaction with demagnetizing structures formed by the lattice. In addition, micromagnetic simulations as well as experiments will illustrate how a tilted external magnetic field affects higher order spin waves in antidot lattices.

To excite low frequency edge modes in the antidot lattice, the sample was excited with a 100 ps broadband pulse that allows to excite multiple frequencies simultaneously. With a Fourier transformation of the experimental data along the temporal axis, each frequency component can be analyzed individually. The same transformation also yields spatially resolved amplitude and phase profiles for each individual frequency.

The spin wave edge mode is highly localized to an area of < 80 nm $\times 130$ nm, which is illustrated by the spin wave amplitude

distribution in Fig. 2(a). The strong localization can be explained by the reduction of the local effective field due to the demagnetizing field formed by the antidot lattice. The reduction of the local effective magnetic field lowers the local resonance frequency,[2] which traps the edge mode inside of a potential well.[20]

A dynamic representation of the 2.0 GHz spin wave component measured with TR-STXM is displayed in Fig. 2(b). The amplitude of the spin wave is given by color saturation while the relative phase is represented by the respective color. The edge mode does not have a uniform temporal phase along the antidot edge but exhibits a phase evolution. This indicates that the edge mode inherits its characteristics from a propagating spin wave mode, which got trapped in a potential well formed in the vicinity of the antidot. The phase gradient, shown as white arrows in Fig. 2(b), represents the propagation direction of the spin wave. This indicates that the wave vector $\vec{k}$ is perpendicular to the magnetization. Hence, the localized edge mode derives from a Damon–Eshbach spin wave.[25,39]

The phase shift of the edge mode depends on both, the excitation as well as the local resonance frequency. While the excitation frequency does not vary as a function of position, the resonance frequency depends on the magnitude of the local field, and hence on the magnitude and direction of the demagnetizing field, which is highly inhomogeneous in the vicinity of the antidot. Since the phase shift is a function of the local resonance frequency, which in turn depends on the position, the phase shift exhibits a spatial variation.

Figure 3(a) displays a propagating, Damon–Eshbach type spin wave mode at 3.0 GHz and 30 mT, which carries significant amplitude across the antidot lattice. Reducing the excitation frequency to 2.4 GHz does not only result in quantitative but also qualitative changes of the spin wave pattern. The more complex pattern is shown in the enlargement in Fig. 3(b). It turns out, this pattern can be deconvoluted into a propagating channel mode and a mode indicated by the white lines. From now, we will refer to the latter one as a dragonfly mode since the white overlay shows similarities to the shape of a dragonfly. A simulated illustration is displayed in the supplementary material (Figs. S1 and S4).

The dragonfly mode starts with magnetization oscillations at the edges and follows the demagnetizing structure. The phase of the propagating channel mode continuously changes during propagation perpendicular to the magnetic field, as shown in Fig. 3(c). The dragonfly mode lags approximately $3\pi/4$ behind the channel mode at their respective position. This suggests that the dragonfly mode acts as a local oscillator that is driven by the propagating mode. Hence, the energy is not transmitted directly from the RF-antenna to the dragonfly mode but needs the channel mode as a mediator that agrees well with previous findings of spin waves interacting with antidots.[5]
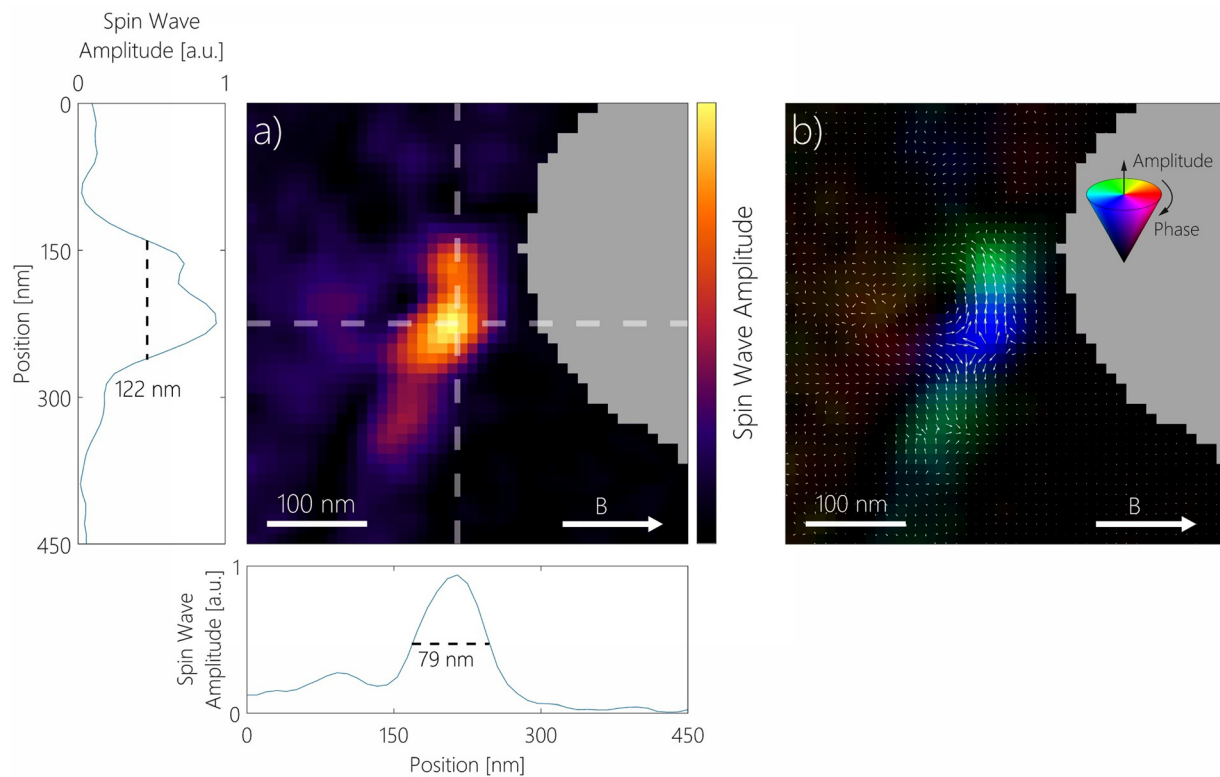
FIG. 2. TR-STXM measurements of a localized edge mode below the microstrip antenna: (a) two-dimensional distribution of the spin wave amplitude at 2.0 GHz and 20 mT after excitation with a 100 ps broadband pulse. The position of the antidot is shown as a gray overlay. Additionally, amplitude profiles through the maximum are displayed next to the plot. (b) Two-dimensional distribution of the spin wave phase (shown as hue) and amplitude (shown as color saturation). The phase gradient is illustrated by white arrows to indicate the propagation direction of the spin waves.
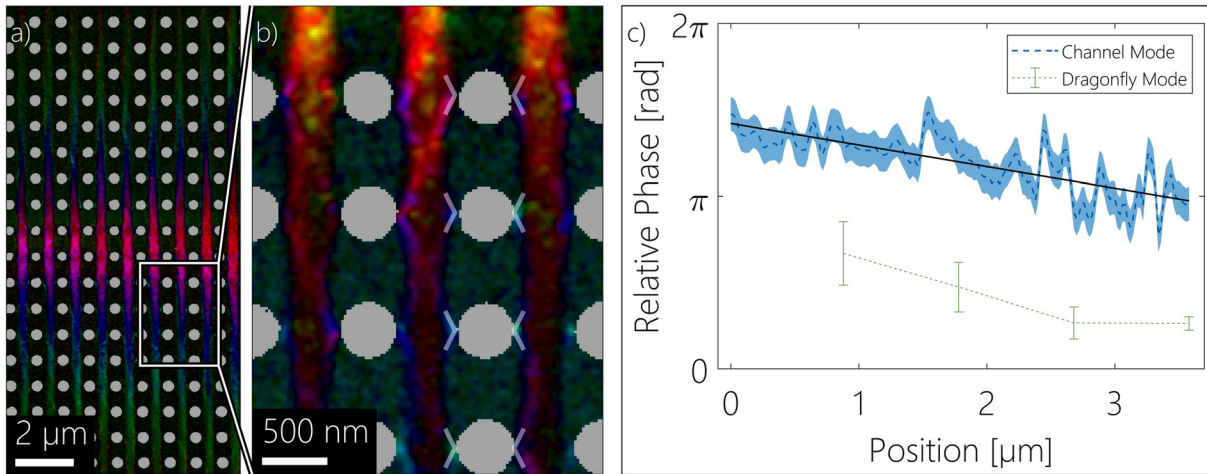
FIG. 3. Two-dimensional distribution of the spin wave phase and amplitude at (a) 3.0 GHz and (b) 2.4 GHz in a magnetic field of 30 mT during continuous wave excitation obtained from TR-STXM measurements. The magnetic field is applied parallel to the antenna. The position of the antidots is shown as gray overlay. The spin wave pattern can be deconvoluted into a propagating Damon–Eshbach wave in each channel and a dragonfly mode, which is indicated by the white transparent overlay next to four of the antidots. A simulated example of a similar mode is illustrated in the supplementary material (supplementary material Fig. S1). Furthermore, (c) displays the spatial phase variation during propagation. The channel mode is represented in blue and black (linear fit), while the dragonfly modes are represented by four green measurement points. The dragonfly mode lags behind the propagating mode indicating its character of a driven oscillation.

Therefore, this represents a possible way to drive local oscillations by a non-localized, propagating mode. Due to its driven nature, the dragonfly mode mimics a spatial phase variation and is sustained by a propagating spin wave mode.

Micromagnetic simulations were performed to get a deeper understanding of the nature of the system at small tilting angles of the external magnetic field. Simulated dispersion relations are shown in Figs. 4(a)–4(c) for three different angles between the external field and the microstrip antenna (0°, 2°, and 4°).

As it turns out the dispersion relation of the system strongly changes its behavior already for slight tilt angles. Due to the perturbation of the magnetization caused by the antidot edges, the system is massively influenced by the resulting demagnetization pattern. This pattern continuously changes with increasing tilt angle (supplementary material Fig. S2) and drastically influences the dispersion relation.

The edge mode band located between 0.5 and 2 GHz gets more narrow for higher field angles, drastically reducing its frequency range. The propagating modes change their frequency response by shifting to higher excitation frequencies. When taking a closer look at the 4° dispersion, it can even be seen that the tilted field geometry not only shifts existing modes but also causes a new mode to appear slightly above 3 GHz (black arrow). Not only is this mode not visible for lower field tilts, it also possesses a negative slope at the Brillouin zone center, typically seen for backward-volume-like spin waves. Nevertheless, this spin wave mode does not directly correspond to a pure propagating spin wave but to a combination of asymmetric channel and edge mode. An example of this mode is displayed in Fig. 4(d). For this illustration, all k-vector components are included in the illustration.

It can be seen that the amplitude of the mode located close to the antidots (white arrow) is not in phase but experiences a phase shift
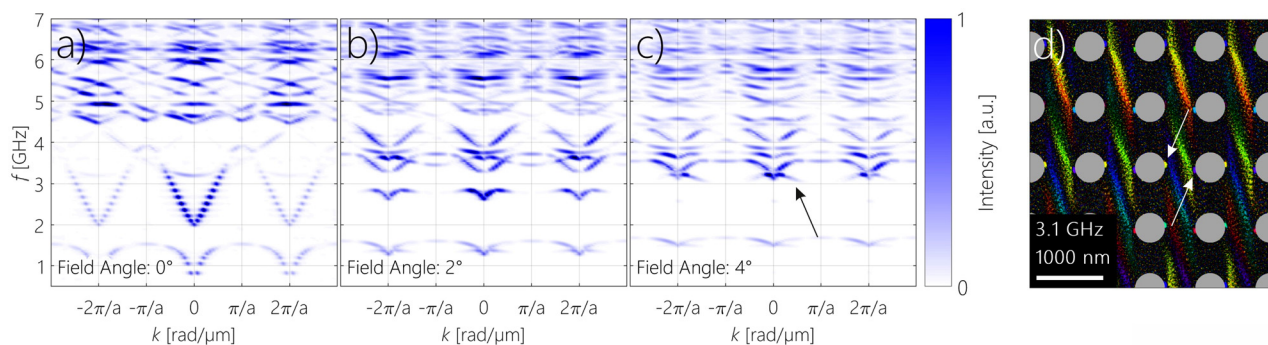
FIG. 4. Changes of the magnonic band structure with slightly tilted magnetic field: (a)–(c) simulated spin wave dispersion relation for an applied field of 25 mT at tilt angles between 0° and 4°. (d) Example plot of a spin wave pattern located within the emerging asymmetric branch at 4° field tilt. Amplitude is represented by color saturation, whereas the relative phase is illustrated by the color.

that is in contrast to conventional symmetric edge modes. This is due to the phase of the channel mode being different on the left and the right sides of the channel, causing a difference in the phase of the driven oscillation at the antidot edges. This asymmetric mode is not excited for smaller tilt angles since the microstrip antenna generates a uniform magnetic field across the channels, which can only couple to symmetric spin waves in the case of a horizontally aligned magnetic field. Even slight tilting breaks the symmetry allowing for excitation of asymmetric waves.

It should be noted that the field is rotated around the sample while the antenna remains oriented along the horizontal axis. Nevertheless, the tilted field makes the excitation of modes that are quantized across the channel quite efficient, thus providing nonzero k-components along the direction of the antenna.

The existence of such asymmetric modes is not obvious and represents an unexpected transformation of the band structure under a tilted external field. In particular, their frequency decreases with increasing k-vector, in contrast to other modes. Since they are located just above a bandgap, this results in them reaching into the otherwise empty bandgap between the symmetric edge modes and the fundamental mode. Although we do not have access to fully conclusive experimental evidence, we have experimental results that strongly indicate the existence of asymmetric oscillations. An illustration is included in the supplementary material (Fig. S3).

To mimic a magnetic field rotation, the sample was mounted slightly tilted with respect to the magnetic field. The tilt of the external magnetic field affects the spin wave dynamics drastically. As seen in Fig. 5, the tilting of the applied field (20 mT) breaks the symmetry of the system, which causes the spin wave to lose its symmetry axis along the propagation direction (cf. Neusser et al.[31] for large tilt angles). Instead the spin waves tend to form tilted zones of maximum amplitude along the channel connecting two opposite antidots as illustrated by the dashed white lines in Figs. 5(a) and 5(c). The amplitude maxima and node-like behavior indicate that the spin waves tend to form standing spin waves between the antidots. For increasing frequency, the amount of nodes increases until the resolution of the measurement does not succeed at resolving individual nodes anymore (6.1 GHz). Increasing the frequency leads to standing spin waves only underneath the antenna. Almost all spin wave energy is now channeled into standing spin waves located between the antidots, outside of the guiding channel.

The experimental results are a nice illustration of the rich nature of spin waves trapped in antidot lattices. The spin wave behavior continuously changes with increasing frequency, while different frequency ranges emphasize different aspects of the wave. It also nicely displays that for some frequencies, the spin waves can only be represented by a superposition of traveling waves with a continuous phase gradient as well as standing spin wave patterns between the individual holes.

The simulations, performed at a tilt angle of 4° and an external field of 25 mT, are able to reproduce the experimental results almost perfectly over a large range of frequencies (Fig. 5). The slight field discrepancy is caused by a non-perfect magnetic field calibration in the experiment. The simulation does not only match the spin wave shape but also operates at almost the same frequencies as the experiment. In the simulations, we find that some modes existing in the lattice cannot be represented by single mode profiles but instead consist of a superposition of multiple individual modes.

Experiment   Simulation
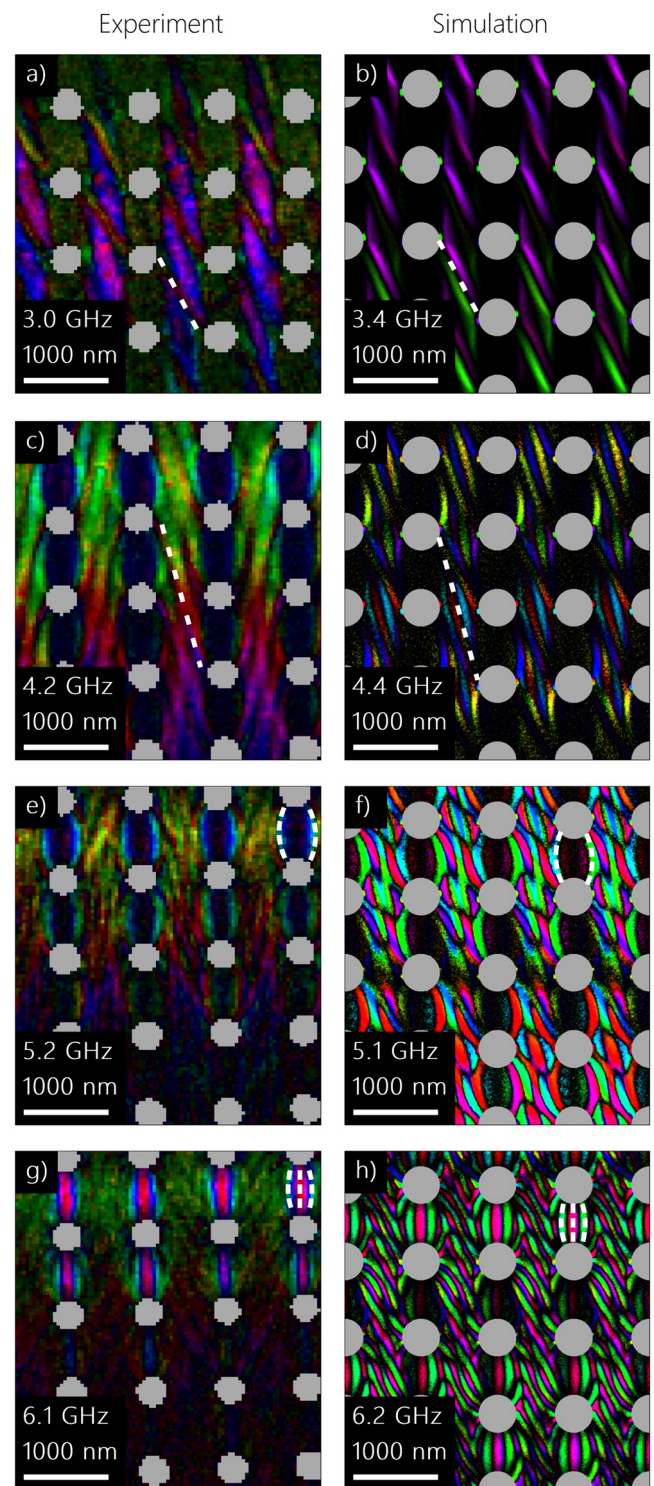
FIG. 5. Comparison of experiment (20 mT, left column) and simulations (25 mT, right column) over a large range of frequencies with the external field direction slightly tilted by 4°. The slight field discrepancy is caused by a non-perfect magnetic field calibration (few mT) in the experiment.

In particular, as shown in Figs. 5(a)–5(d), the simulation is able to capture the tilt of the spin wave modes and reproduces the standing spin wave pattern between the antidots. The dashed white lines indicate the mode tilt angle that matches well for experiment and simulation. The simulation is also able to recreate the amount of nodes between two neighboring antidots.

Although the simulation overestimates the spin wave amplitude within the spin wave channel for higher frequencies, the overall shape of the spin wave pattern is well-captured. Examples of the most dominant features are highlighted by white dashed lines in Figs. 5(e)–5(h).

In summary, we reported on three different types of propagating modes and edge modes near nano-scaled antidots by means of time-resolved scanning transmission x-ray microscopy and micromagnetic simulations. The combination of magnetic resolution paired with time resolved imaging allows observing edge modes that are confined to an area of $< 80\,\mathrm{nm} \times 130\,\mathrm{nm}$. The phase sensitivity of STXM enables us to visualize the edge mode phase propagation, which indicates a Damon–Eshbach-like character.

Increasing the excitation frequency allows us to excite propagating modes traveling down the spin wave channel. High resolution movies reveal that the demagnetization structures near the antidots result in dragonfly like modes. Their fixed phase relation to the channel mode suggests that the oscillation of the dragonfly mode is a driven oscillation fed by the propagating channel mode. This demonstrates a possibility to excite localized modes by a non-local, propagating spin wave.

Rotating the external magnetic field by only 4° reveals asymmetric modes in the simulations, which cannot be excited at smaller tilt angles. This asymmetric branch is an additional feature in the dispersion relation due to the broken symmetry. We illustrated that the simulations are able to recreate the tilted standing spin wave pattern between antidots while also reproducing predominant features of the experiment over a large range of frequencies. We expect the presented results to be an important step toward utilization and manipulation of a rich family of spin wave modes in magnonic crystals.

See the supplementary material that includes an illustration of a simulated dragonfly mode (Fig. S1), simulated magnetization patterns for different field angles (Fig. S2), experimental indications for asymmetric spin wave modes (Fig. S3), and simulated results of the dragonfly and asymmetric mode for different geometrical parameters (Fig. S4).

DATA AVAILABILITY

The data that support the findings of this study are available from the corresponding author upon reasonable request.

REFERENCES

[1] V. V. Kruglyak, S. O. Demokritov, and D. Grundler, J. Phys. D **43**(26), 260301 (2010).

[2] B. Lenk, H. Ulrichs, F. Garbs, and M. Münzenberg, Phys. Rep. **507**(4–5), 107–136 (2011).

[3] M. Krawczyk and D. Grundler, J. Phys.: Condens. Matter **26**(12), 123202 (2014).

[4] A. V. Chumak, V. I. Vasyuchka, A. A. Serga, and B. Hillebrands, Nat. Phys. **11**(6), 453–461 (2015).

[5] F. Groß, M. Zelent, N. Träger, J. Förster, U. T. Sanli, R. Sauter, M. Decker, C. H. Back, M. Weigand, K. Keskinbora, G. Schütz, M. Krawczyk, and J. Gräfe, ACS Nano **14**(12), 17184–17193 (2020).

[6] Z. K. Wang, V. L. Zhang, H. S. Lim, S. C. Ng, M. H. Kuok, S. Jain, and A. O. Adeyeye, Appl. Phys. Lett. **94**(8), 083112 (2009).

[7] Z. K. Wang, V. L. Zhang, H. S. Lim, S. C. Ng, M. H. Kuok, S. Jain, and A. O. Adeyeye, ACS Nano **4**(2), 643–648 (2010).

[8] H. Ulrichs, B. Lenk, and M. Münzenberg, Appl. Phys. Lett. **97**(9), 092506 (2010).

[9] F. Lisiecki, J. Rychły, P. Kuświk, H. Głowiński, J. W. Kłos, F. Groß, I. Bykova, M. Weigand, M. Zelent, E. J. Goering, G. Schütz, G. Gubbiotti, M. Krawczyk, F. Stobiecki, J. Dubowik, and J. Gräfe, Phys. Rev. Appl. **11**(5), 054003 (2019).

[10] F. Lisiecki, J. Rychły, P. Kuświk, H. Głowiński, J. W. Kłos, F. Groß, N. Träger, I. Bykova, M. Weigand, M. Zelent, E. J. Goering, G. Schütz, M. Krawczyk, F. Stobiecki, J. Dubowik, and J. Gräfe, Phys. Rev. Appl. **11**(5), 054061 (2019).

[11] F. Groß, N. Träger, J. Förster, M. Weigand, G. Schütz, and J. Gräfe, Appl. Phys. Lett. **114**(1), 012406 (2019).

[12] J. Gräfe, M. Weigand, B. Van Waeyenberge, A. Gangwar, F. Groß, F. Lisiecki, J. Rychly, H. Stoll, N. Träger, J. Förster, F. Stobiecki, J. Dubowik, J. Klos, M. Krawczyk, C. H. Back, E. J. Goering, G. Schütz, H.-J. M. Drouhin, J.-E. Wegrowe, and M. Razeghi, Proc. SPIE **11090**, 1109025 (2019).

[13] J. Förster, J. Gräfe, J. Bailey, S. Finizio, N. Träger, F. Groß, S. Mayr, H. Stoll, C. Dubs, O. Surzhenko, N. Liebing, G. Woltersdorf, J. Raabe, M. Weigand, G. Schütz, and S. Wintz, Phys. Rev. B **100**(21), 214416 (2019).

[14] N. Träger, P. Gruszecki, F. Lisiecki, F. Groß, J. Förster, M. Weigand, H. Glowinski, P. Kuswik, J. Dubowik, M. Krawczyk, and J. Gräfe, Nanoscale **12**(33), 17238–17244 (2020).

[15] A. V. Chumak, A. A. Serga, B. Hillebrands, and M. P. Kostylev, Appl. Phys. Lett. **93**(2), 022508 (2008).

[16] S. Neusser and D. Grundler, Adv. Mater. **21**(28), 2927–2932 (2009).

[17] S. Mamica, X. Zhou, A. Adeyeye, M. Krawczyk, and G. Gubbiotti, Phys. Rev. B **98**(5), 054405 (2018).

[18] E. K. Semenova and D. V. Berkov, J. Appl. Phys. **114**(1), 013905 (2013).

[19] R. Zivieri, S. Tacchi, F. Montoncello, L. Giovannini, F. Nizzoli, M. Madami, G. Gubbiotti, G. Carlotti, S. Neusser, G. Duerr, and D. Grundler, Phys. Rev. B **85**(1), 012403 (2012).

[20] J. Jorzick, S. O. Demokritov, B. Hillebrands, M. Bailleul, C. Fermon, K. Y. Guslienko, A. N. Slavin, D. V. Berkov, and N. L. Gorn, Phys. Rev. Lett. **88**(4), 047204 (2002).

[21] S. Neusser, B. Botters, and D. Grundler, Phys. Rev. B **78**(5), 054406 (2008).

[22] M. Kostylev, G. Gubbiotti, G. Carlotti, G. Socino, S. Tacchi, C. Wang, N. Singh, A. O. Adeyeye, and R. L. Stamps, J. Appl. Phys. **103**(7), 07C507 (2008).

[23] C. L. Hu, R. Magaraggia, H. Y. Yuan, C. S. Chang, M. Kostylev, D. Tripathy, A. O. Adeyeye, and R. L. Stamps, Appl. Phys. Lett. **98**(26), 262508 (2011).

[24] S. Tacchi, B. Botters, M. Madami, J. W. Kłos, M. L. Sokolovskyy, M. Krawczyk, G. Gubbiotti, G. Carlotti, A. O. Adeyeye, S. Neusser, and D. Grundler, Phys. Rev. B **86**(1), 014417 (2012).

[25] S. Tacchi, P. Gruszecki, M. Madami, G. Carlotti, J. W. Klos, M. Krawczyk, A. Adeyeye, and G. Gubbiotti, Sci. Rep. **5**, 10367 (2015).

[26] M. Zelent, N. Tahir, R. Gieniusz, J. W. Kłos, T. Wojciechowski, U. Guzowska, A. Maziewski, J. Ding, A. O. Adeyeye, and M. Krawczyk, J. Phys. D **50**(18), 185003 (2017).

[27] V. V. Kruglyak, A. Barman, R. J. Hicken, J. R. Childress, and J. A. Katine, Phys. Rev. B **71**(22), 220409–22040R (2005).

[28] V. V. Kruglyak, P. S. Keatley, R. J. Hicken, J. R. Childress, and J. A. Katine, J. Appl. Phys. **99**(8), 08F306 (2006).

[29]B. B. Maranville, R. D. McMichael, S. A. Kim, W. L. Johnson, C. A. Ross, and J. Y. Cheng, J. Appl. Phys. **99**(8), 08C703 (2006).

[30]B. B. Maranville, R. D. McMichael, and D. W. Abraham, Appl. Phys. Lett. **90**(23), 232504 (2007).

[31]S. Neusser, G. Duerr, H. G. Bauer, S. Tacchi, M. Madami, G. Woltersdorf, G. Gubbiotti, C. H. Back, and D. Grundler, Phys. Rev. Lett. **105**(6), 067208 (2010).

[32]B. Rana, D. Kumar, S. Barman, S. Pal, Y. Fukuma, Y. Otani, and A. Barman, ACS Nano **5**(12), 9559–9565 (2011).

[33]H. T. Nembach, J. M. Shaw, C. T. Boone, and T. J. Silva, Phys. Rev. Lett. **110**(11), 117201 (2013).

[34]C. Cheng, W. Cao, and W. E. Bailey, J. Magn. Magn. Mater. **424**, 12–15 (2017).

[35]F. Guo, L. M. Belova, and R. D. McMichael, Phys. Rev. Lett. **110**(1), 017601 (2013).

[36]S. Tacchi, G. Duerr, J. W. Klos, M. Madami, S. Neusser, G. Gubbiotti, G. Carlotti, M. Krawczyk, and D. Grundler, Phys. Rev. Lett. **109**(13), 137202 (2012).

[37]A. Vansteenkiste, J. Leliaert, M. Dvornik, M. Helsen, F. Garcia-Sanchez, and B. Van Waeyenberge, AIP Adv. **4**(10), 107133 (2014).

[38]D. Nolle, M. Weigand, P. Audehm, E. Goering, U. Wiesemann, C. Wolter, E. Nolle, and G. Schütz, Rev. Sci. Instrum. **83**(4), 046112 (2012).

[39]R. W. Damon and J. R. Eshbach, J. Phys. Chem. Solids **19**(3–4), 308–320 (1961).